The Impact of Dysprosium Ions as a Dopant on Linear and Nonlinear Optical Dispersion Parameters in a-Se Thin Film

Fathy A. Abdel-Wahab[*], Heba Abdel Maksoud

Physics Department, Faculty of Science, Ain Shams University, Cairo, Egypt

Abstract   Thin films of un-doped and doped a-Se with Dysprosium rare earth ions have been prepared by thermal evaporation technique. The optical transmission spectra of the investigated films have been measured in a wide spectral range and used to calculate the linear optical constants together with the optical energy gap of studied films. The observed decrease in the values of the energy gap against the increase of the Dysprosium (Dy) content in a-Se films has been explained using Mott and Davis Model and in terms of electronegativity difference of the constituent atoms. Furthermore, the dispersion of nonlinear parameters such as second order refractive index and nonlinear absorption coefficient (two-photon absorption coefficient) of investigated films are presented and discussed.

Keywords   Dysprosium ions, Se doped Dy, Optical transmittance, Optical energy gap, Second order refractive index

1. Introduction

Rare earth Dysprosium (Dy) ions doped glasses are very interesting due to its application as solid-state laser materials and as a suitable candidate for analysing the energy-efficient luminescent materials [1, 2]. Furthermore, as a result of presence of active f electron shell, which is very sensitive to the surrounding atoms of the host environment, in the electronic configuration of Dy it can provide an emission at 1.3 μm due to the $^6F_{11/2}$, $^6H_{9/2} \rightarrow {}^6H_{15/2}$ transitions [3]. In addition, due to its absorption band at approximately 800 nm, it could be excited using a cheap commercial laser diode.

In contrast, the structure of a-Se consists of flat and straight zigzag chains (Se_n) and eight membered rings (Se_8). This structure makes a-Se characterizes by existence of localized states in its energy gap which are created due to presence of structural dangling bond defects and absence of long range order [4-6]. Also, the structural disorder of a-Se makes it and its chalcogenide alloys to have a high thermal stability, high degree of covalent bonding, large refractive index and optical transparency in the infra-red (IR) spectral regions up to 10 μm. Furthermore, due to its high rare earth solubility, high emission   quantum efficiency   and the low

phonon energy it could be used as a suitable host medium for Dy ions to enhance its mid-IR laser emission [7, 8]. Consequently, the investigation of the optical properties of doped a-Se with Dy ions is very important to improve the performance of Laser emission [9]. In the previous work [10], the study of Selenium films was intended to have a comprehensive understanding over the influence of Dysprosium (Dy) ion dopant on the ac conductivity and dielectric parameters of a-Se films. The present aims to gain a better investigation on the effect of doping with Dy on the optical dispersion relations of the complex dielectric constant, optical energy gap and material dispersion. Furthermore, the effect of doping of a-Se with Dy ions on second order refractive index and two photons absorption are calculated and discussed.

2. Experimental Details

Bulk selenium samples doped with Dysprosium with ratios 0.008 and 0.01 at. % are prepared by mixing suitable proportions of Se and Dy, of purity 5 N, in a silica tube sealed at 10^{-5} Torr. The mixture was heated in an electric furnace up to 950℃ and kept at that temperature for 9 h. The obtained bulk ingots are used as source material to prepare thin films by the thermal evaporation technique. More details about bulk and thin films preparation of Se doped Dy is given elsewhere [10]. After evaporation, the thickness of the fresh films was accurately determined by an optical interference method and is found to be in the range of 750-804 nm.

The structural phase of as-prepared thin film samples has been identified using an X-ray diffraction pattern (XRD) computerized system (model: Philips EXPERT-MPDUG PW-3040 diffractometer with Cu Ka radiation source). Computer-aided two-beam spectrophotometer of type Shimadzu- 3101PC UV–VIS–NIR, is used to record the optical transmittance (T) as a function of wavelength (λ) for the investigated films. A resolution limit of 0.2 nm and a sampling interval of 2 nm were utilized for recording the different measuring points. The accuracy of measuring $T(\lambda)$ is 0.003 with the incident beam at normal incidence to the film surface. The optical measurements were carried out at room temperature in the spectral region of 500–2500 nm.

3. Results and Discussion
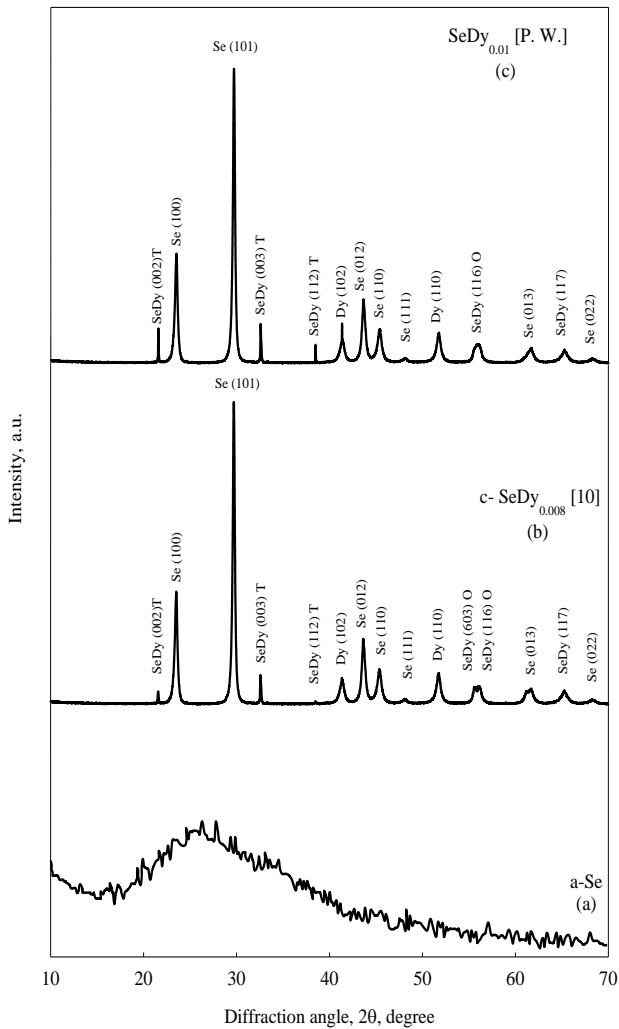
Figure 1. XRD pattern for a-Se (a), c-SeDy$_{0.008}$ [10] (b) and the present work [P. W.] of SeDy$_{0.01}$ (c) thin films. It should be noted that the diffraction pattern of c-SeDy$_{0.008}$ [10] is added to the figure for the sake of comparison

Figure 1 shows the recorded XRD patterns for the studied as-prepared a-Se, previous work of SeDy$_{0.008}$ films [10], and the present work [P.W.] of Se films doped with 0.01 at. %

with Dy. In this figure, the XRD pattern of the fresh Se films reflects its amorphous nature. The observed diffraction peaks in case of Se doped with 0.008 at. % Dy [10] means the growth of crystalline phase on the expense of amorphous state. This crystalline phase consists of mixed phases of elemental Se, Dy and tetragonal and orthorhombic structures of SeDy as shown in Figure 1. Furthermore, increasing the Dy content in a-Se up to 0.01 at. % increased the intensity of the diffraction peaks for (102) of Dy and (002), (003) and (112) phases for SeDy which means that increasing the growth of crystalline zones in SeDy$_{0.01}$ as shown in Figure 1.

3.1. Linear Optical Dispersion

The linear optical constants such as refractive index (n), extinction coefficient (k) and optical energy gap, E_g, are considered as a key parameter for optimizing optical properties of a given optical application [11]. The measured optical transmission against wavelength are used evaluate the linear constants n and k for un-doped and Dy doped Se films using Swanepoel method [12-14].
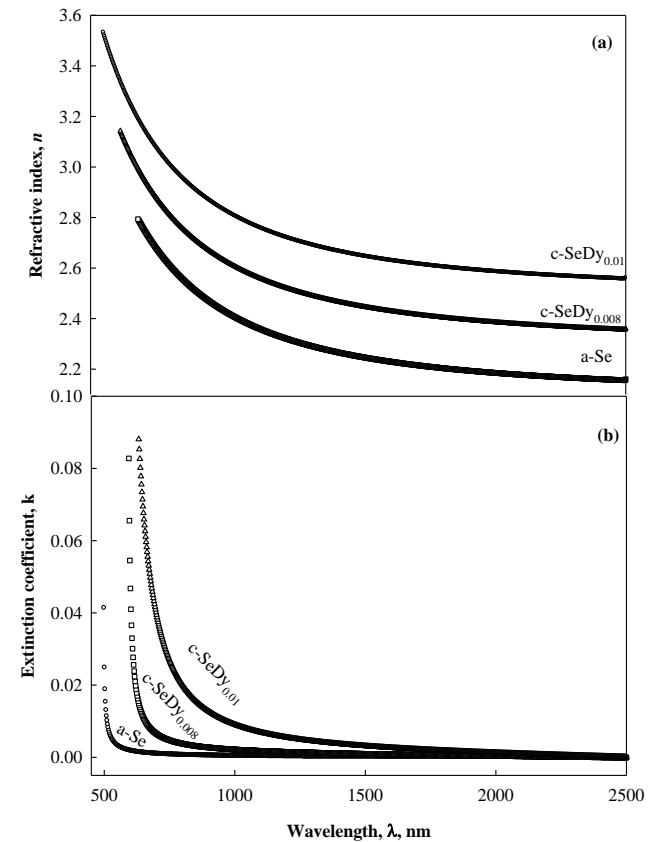
Figure 2. Variation of refractive index (n) (a) and extinction coefficient (k) (b) with wavelength (λ) for the studied a-Se, c-SeDy$_{0.008}$ and c-SeDy$_{0.01}$ thin films

Figure 2 shows the dependence of the calculated linear optical constants n and k, on the applied wavelength and compositions of the investigated samples. In Figure 2, the calculated values of n and k show a decrease against wavelength which is due to the normal optical dispersion of

the studied films. Indeed, the figure shows also an increase of n and k against the increase of Dy ratio in the network of a-Se. This behaviour can be interpreted as follows: due to the electronic configuration of Dysprosium [Xe] $4f^{10}6s^2$ each Dy atom provides a-Se network with two electrons and transform to Dy^{2+} ion. Consequently, an increase in the density of dipoles and electrons in Selenium network is expected as calculated in Table 1 of the present work. In Table 1 the density of dipoles increases from 5.71×10^{50} $cm^{-3}.Kg^{-1}$ (for a-Se) up to 6.25×10^{50} $cm^{-3}.Kg^{-1}$ (for c-SeDy$_{0.01}$). The increased density of oscillating dipoles and its associated density of electrons increases the electronic polazibility which controls not only the refractive index but also the optical absorption of the studied samples [15].

Figure 3 shows refractive index as a function of composition for the investigated a-Se doped with Dy rare earth ions films together with those published in literature at $\lambda= 1.3$ µm using different preparation techniques. The general trend of the function is the increase of n against Dy content ratio in at. %. However, the discrepancy among the data published by assorted authors is attributed to the variation in the preparation techniques used in formulating the studied materials in each reference besides the dependence of the properties of chalcogenides on its thermal history. In [3] bulk samples are prepared by conventional melt quenching technique for the mixture of the constituent elements. The obtained ingots are annealed at its glass transition temperature before any measurements. Furthermore, in [16] the obtained melt quenched ingots are used as a source material to prepare thin film samples using KrF excimer laser operating at 248 nm.
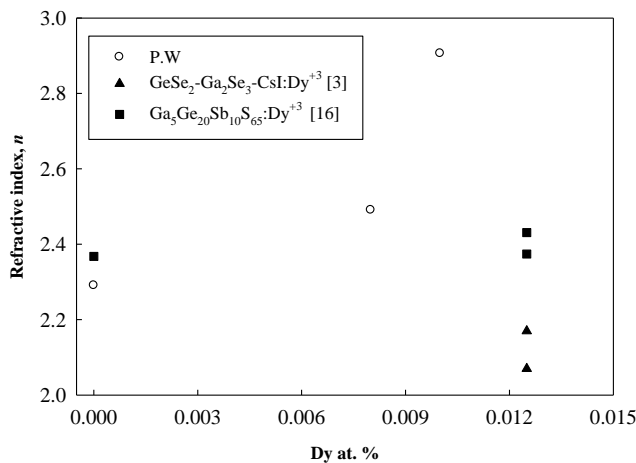
Figure 3. Variation of refractive index as a function of the doped Dy rare earth ions in at. % for the present work [P. W.] with those published in the literature such as GeSe$_2$-Ga$_2$Se$_3$-CsI [3] and Ga$_5$Ge$_{20}$Sb$_{10}$S$_{65}$ [16]

The dependence of the optical absorption coefficient (α), calculated using values of the extinction coefficient in Figure 2a, on the incident photon energy of the investigated films are shown in Figure 4. This figure confirms that for all studied samples the value of α increases against photon

energy in exponential trend and shifted towards lower energy as doping rate increases in the structural network of a-Se films. This shift indicates that the absorption edge decreases in energy (red shift in wavelength) against the increase of doping level of Dy.

Each curve recognized in Figure 4, could be divided into two different regions [17, 18].
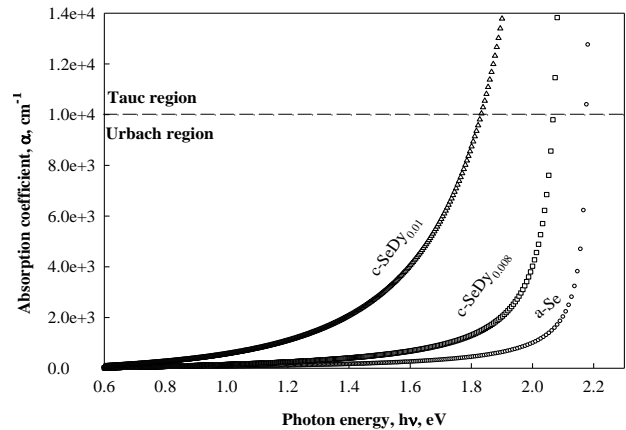
Figure 4. The calculated absorption coefficient (α) as function of photon energy ($h\nu$) for the studied films. The dashed horizontal line differentiates between the Tauc and Urbach regions

The first region is for the high absorption, namely for $\alpha(h\nu) > 10^4$ cm^{-1} (Tauc region). The optical absorption in this region could be described by Tauc's relation [17]:

$$\alpha(h\nu) = A(h\nu - E_g)^r \qquad (1)$$

where A is constant, E_g the optical band gap and $r=1/2$ as well as 2 for direct and indirect transitions in sequence. According to equation (1), the dependence of $(\alpha h\nu)^{1/r}$ versus $h\nu$ is shown in Figure 5, for both values of r. For each composition, the energy gap E_g are calculated by fitting the function $(\alpha h\nu)^{1/r} =f(h\nu)$, locally point by point to linear regression line and extrapolating to y=0 yields the value of E_g. The results are given in Table 1, as function of the film compositions. According to Table 1, it is observed that the value of optical band gap E_g decreases against increase of Dy content through considered range of doping 0.008-0.01 at. % of Dy.

The decrease of E_g against the increase of Dy content in the structural network of a-Se can be explained using the electronegativity of the elements involved. The electronegativity of Se and Dy are 2.55 and 1.22 respectively. The valance band of a-Se contains the lone pair p-electrons and addition of an element with lower electronegativity (Dy) to a higher electronegative element (Se) may raise the energy of lone pair states, which is further responsible for the broadening of the valance band inside the forbidden gap and leads to band tailing and hence band gap shrinkage [19].

The second region in Figure 4, with $\alpha(h\nu) < 10^4$ cm^{-1} (Urbach region), where the absorption coefficient presents a roughly exponential behavior:

$$\alpha(h\nu) = \alpha_e \exp\left(\frac{h\nu}{E_u}\right) \tag{2}$$

Where α_e is a constant and E_u is an energy which is often interpreted as the width of the tail of localized states in the gap region. This relation was first proposed by Urbach [20]. The reciprocal of the slope or width of the exponential edge E_u reflects the width of the localized band tail [21] which is called Urbach energy. It determines the degree of disorder in the semiconductor which is responsible for internal potential fluctuations giving rise to tails of localized states at the band edges. The Urbach energy depends strongly on deposition conditions and annealing, which are likely to influence the disorder and therefore the band tailing [22]. The calculated values of E_u are given in Table 1, as a function of film compositions. These values show a decrease from 0.30 eV for un-doped a-Se film to 0.25 and 0.21eV for doping with 0.008 and 0.01 at. % in sequence. Such decrease in the value of E_u indicates a decrease in the disorder character of a-Se due to the introduction of Dy which is consistent with the obtained structure using XRD for the studied samples shown in Figure 1, consequently, a decrease of E_u is attributed to the crystallized character of the thermally deposited films. Also, the existence of band tail (E_u) that accompanied the localized states in the gap reflects some degree of disorder in the considered semiconductor film.
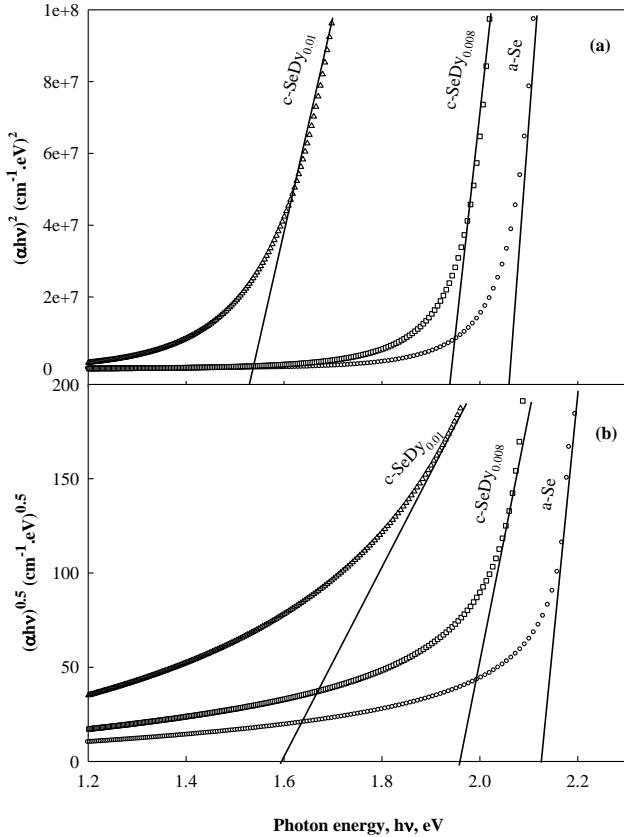
Table 1. The Calculated Values of the Optical Energy Gap, E_g, Urbach Energy, E_u, High Frequency Dielectric Constant, ε_∞, Ratio of the Free Carriers Density to the Free Carrier Effective Mass, N/m^* and Plasma Resonance Frequency, ω_p, as a Function of the Studied Film Compositions

Film Composition	E_g, eV	E_u, eV	ε_∞	$(N/m^*) \times 10^{50}$ (cm^{-3} kg^{-1})	$\omega_p \times 10^{14}$ Hz
a-Se	2.10	0.30	4.91	5.710	1.94
c-SeDy$_{0.008}$	1.96	0.25	5.54	6.079	2.48
c-SeDy$_{0.01}$	1.59	0.21	6.77	6.250	2.87

The complex dielectric constant $\varepsilon^* = \varepsilon_1 - i\varepsilon_2$ of a martial in terms of the linear optical constants, n, and, k, could be written as $\varepsilon_1 = n^2 - k^2$, $\varepsilon_2 = 2nk$ where ε_1 is the real part, while ε_2 is the imaginary part. Figure 6, shows the calculated values of ε_1 and ε_2 of the complex dielectric constant versus the photon energy ($h\nu$) for the present film compositions. Figure 6a, shows nearly exponential increase with photon energy for all investigated samples and nearly has the same trend as $n=f(\lambda)$. On the other hand, ε_2 illustrates a clear exponential increase of ε_2 against ($h\nu$) which has the same behavior as $k=f(h\nu)$.

For a better understanding of the optical behavior of the investigated films, it is necessary to determine some optical parameters such as dispersion of high-frequency dielectric constant and the lattice vibration modes as follows:

In the near infrared spectral region, where the frequency is relatively low, the real ε_1 and imaginary ε_2 parts of the complex dielectric constant can be written as [23]:

$$\varepsilon_1 = \varepsilon_\infty - \frac{e^2}{4\pi^2 c^2 \varepsilon_0} \frac{N}{m^*} \lambda^2, \qquad \varepsilon_2 = \frac{\varepsilon_\infty \omega_p^2}{8\pi^3 c^3 \tau} \lambda^3 \tag{3}$$

where ω_p is the plasma resonance frequency $\omega_p = \left(e^2 N / \varepsilon_0 \varepsilon_\infty m^*\right)^{1/2}$ of all the valence electrons involved in the optical transitions, ε_∞ the high frequency dielectric constant, e electronic charge, c speed of light, ε_o free space constant, N/m^* is the ratio of free carriers density to the free carrier effective mass and τ relaxation time. According to equation (3), plot of ε_1 versus λ^2 and extrapolating the linear part of the plot in the high wavelength region to zero wavelength gives the value of ε_∞ and the slope of this line are used to calculate values of (N/m^*) for the investigated films. The calculated ε_∞, (N/m^*) and ω_p are given in Table 1, as a function of studied film compositions. The value of N/m^* reflects an increase in the free carrier density with the increase of Dy-content which is argued to the metal character of Dysprosium rare earth.

According to the single-effective oscillator model suggested by Wemple and DiDomenico [24], the refractive index could be described by the following relation:

$$n^2 - 1 = \frac{E_0 E_d}{E_0^2 - E^2} \tag{4}$$

where E is the photon energy in eV, E_0 is the single oscillator energy (average oscillator energy for electrons) and E_d is the dispersion energy parameter of the material. For the magnetic chalcogenides such as the present case of Dy doped

Figure 5. Tauc's plots for determining the optical energy gap of direct (a) and indirect (b) transitions for films investigated

Se films, equation (4), could be rewritten as [24]:
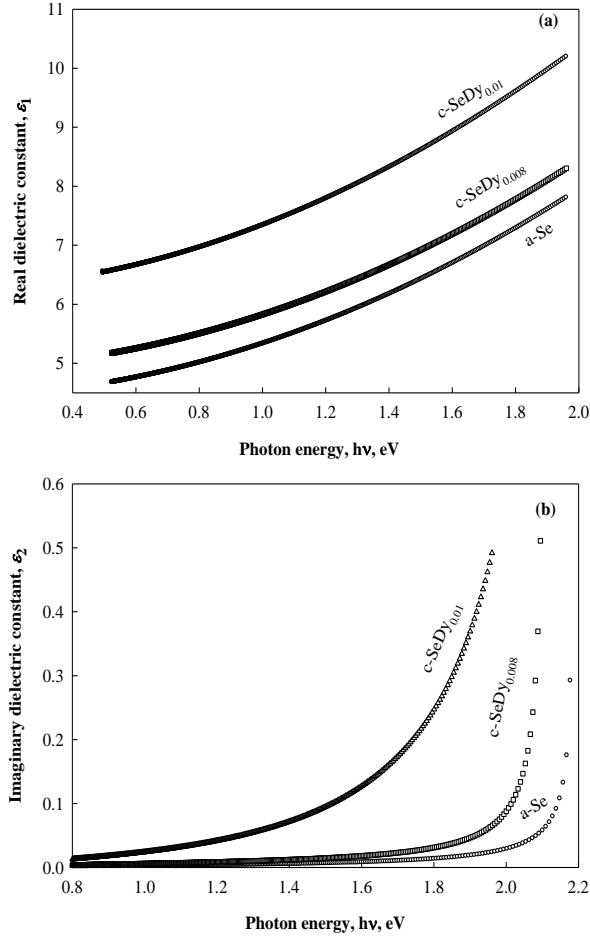
Figure 6. Real (a) and imaginary (b) parts of the dielectric constant versus photon energy for the films investigated

$$n^2 - 1 = \frac{\hat{E}_d \hat{E}_0}{\hat{E}_0^2 - E^2} + \frac{E_d E_0}{E_0^2 - E^2} \qquad (5)$$

Where $\hat{E}_d$, $\hat{E}_0$ applies to $f \rightarrow d$ transitions and E_d, E_0 applies to s, $p \rightarrow d$ transitions. It is straightforward to combine terms in equation (5), and get the following expressions for the equivalent single oscillator parameters $\bar{E}_0$ and $\bar{E}_d$ [24]:

$$\bar{E}_0^2 = \hat{E}_0^2 \left(\frac{1 + \left(E_d / \hat{E}_d\right)\left(\hat{E}_0 / E_0\right)}{1 + \left(E_d / \hat{E}_d\right)\left(\hat{E}_0 / E_0\right)^3} \right) \qquad (6)$$

and

$$\bar{E}_d^2 = \hat{E}_d^2 \left(\frac{\left[1 + \left(E_d / \hat{E}_d\right) \left(\hat{E}_0 / E_0\right)\right]^3}{1 + \left(E_d / \hat{E}_d\right) \left(\hat{E}_0 / E_0\right)^3} \right) \qquad (7)$$

$\bar{E}_0$ is the dispersion energy parameter of the material and is a measure of the strength of interband optical transitions and $\bar{E}_d$ is related to the nearest neighbour cation coordination, anion valency, ioniciy and effective number of dispersion electrons. According to equation (5), Plotting $(n^2-1)^{-1}$ versus the photon energy $(h\nu)^2$ as shown in Figure 7, and fitting the

straight part of the curve in the high energy region allows to obtain from the slope and the intercept values of E_0 and E_d. In the low energy region, the slope and intercept of the straight line yields the values of $\hat{E}_d$ and $\hat{E}_0$. The calculated values of these dispersion parameters are listed in Table 2.

The estimated value of E_0 for a-Se (4.5 eV) is in good agreement with that reported by Wemple [25]. The results indicated that the average value of the single oscillator energy ($\bar{E}_0$) changed to 3.79 eV for c-SeDy$_{0.008}$ and to 4 eV for c-SeDy$_{0.01}$. Such behavior of $\bar{E}_0$ could be attributed to the splitting of the sub-bands $5d(t_{2g}\text{-}e_g)$ by the crystal field and the decrease of this splitting as well as the crystallized nature with increasing Dy-content.
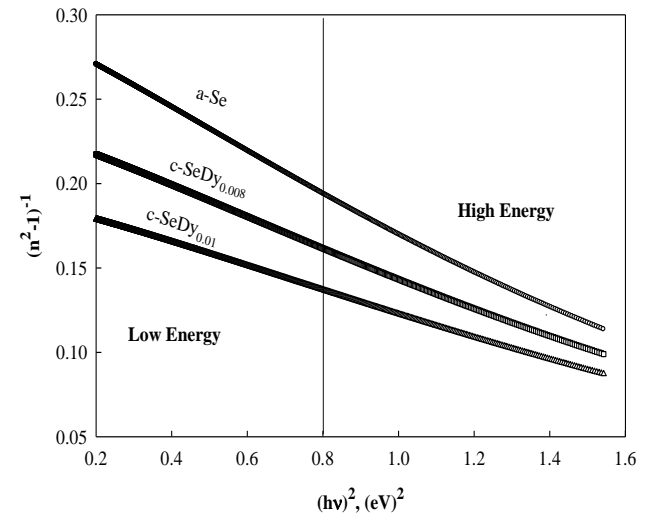
Figure 7. Plots of $(n^2-1)^{-1}$ versus $(h\nu)^2$ for the investigated samples

Table 2. Values of Single Oscillator Energy (E_0, $\bar{E}_0$), Dispersion Energy (E_d, $\bar{E}_d$) Lattice Oscillator Strength (E_l), and Wavelength at Zero Material Dispersion (λ_c) for Investigated Film Compositions

Film Composition	E_0, eV	E_d, eV	$\hat{E}_0$, eV	$\hat{E}_d$, eV	$\bar{E}_0$, eV	$\bar{E}_d$, eV	E_l, eV	λ_c, μm
a-Se	4.50	24.2	---	---	---	---	0.54	1.60
c-SeDy$_{0.008}$	3.74	12.6	2.49	6.34	3.9	8.36	0.36	1.66
c-SeDy$_{0.01}$	3.18	11.6	2.17	5.45	4.0	12.6	0.38	1.74

If the wavelengths much shorter than the phonon resonance, the lattice contribution is given by:

$$n^2 - 1 = \frac{\hat{E}_d \hat{E}_0}{\hat{E}_0^2 - E^2} + \frac{E_d E_0}{E_0^2 - E^2} - \frac{E_l^2}{E^2}, \qquad (8)$$

where E_l is the lattice oscillator strength. Poignant [26] has shown that at long wavelength, where $E^2 << \hat{E}_0^2$ and $E^2 << E_0^2$, a plot of (n^2-1) versus $1/E^2$ approaches a straight line and equation (8), could be written as:

$$n^2 - 1 = \left(\frac{\hat{E}_d}{\hat{E}_0} + \frac{E_d}{E_0} \right) - \frac{E_l^2}{E^2} \qquad (9)$$

The intercept of this line yields the ratio E_d/E_0 at high energy, and $\hat{E}_d/\hat{E}_0$ at low energy, while the slope is $-E_l^2$. The

obtained values of E_l are given in Table 2. The tabulated values of E_l shows variation from 0.54 eV for a-Se to 0.36 eV for c-SeDy$_{0.008}$, and 0.38 eV for c-SeDy$_{0.01}$ respectively.

The material dispersion $M(\lambda)$ could be expressed in terms of the refractive index, n, as:

$$M(\lambda) = \frac{\lambda}{c}\left(\frac{d^2n}{d\lambda^2}\right) \tag{10}$$

Differentiating equation (8), w.r.t λ yields the materials dispersion as a function of $\bar{E}_0$ and $\bar{E}_d$. as follows [25]:

$$M(\lambda) = 1.54\times10^4\,\frac{\bar{E}_d/\bar{E}_0^3}{n\lambda^3} - 2.17\times10^3 E_l^2\,\frac{\lambda}{n} \quad (ps\,nm^{-1}km^{-1}) \tag{11}$$

Figure 8 shows the graphical relation of the calculated $M(\lambda)$ versus wavelength. The wavelength at which $M = 0$, and the obtained results are given in Table 2, as a function of film compositions. Similarly, the value of λ_c can be calculated from the Wemple's three-parameter formula [25]:

$$\lambda_c = 1.63\left(\frac{\bar{E}_d}{\bar{E}_0^3\bar{E}_l^2}\right)^{\frac{1}{4}} \tag{12}$$

Nevertheless, the observed variation of λ_c indicates that the introduction of Dy atoms in a-Se causes a shift of the material dispersion $M(\lambda)$ towards higher wavelengths. Such a red shift represents an important parameter to improve the operational conditions and performance of optical fibers [27, 28]. Indeed, the listed values of material dispersion in Table 2, show that the pumping of optical signals in the Selenium chalcogenide fibers at zero material dispersion wavelength (ZMD) could be tuned by increasing the doping ratio of Dy [29, 30].
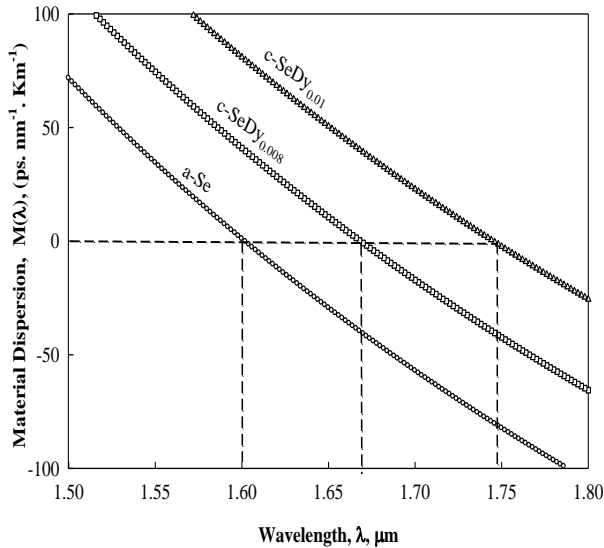
Figure 8.   Variation of the material dispersion versus wavelength for the studied films

3.2. Non-Linear Optical Dispersion

The microscopic nonlinear properties of the chalcogenide semiconductors have investigated through the determination of second-order refraction index, n_2 and nonlinear absorption coefficient, β where n_2 and β are expressed as

$$n_t = n + n_2I \tag{13}$$

and $\alpha(I) = \alpha + \beta I$, where I is the incident intensity, n_t is the total refractive index and n represents the weak-field refractive index (linear refractive index). The second-order index of refraction, n_2 is required for soliton propagation in the optical telecommunication fibers and used in all optical switching schemes.

Boling et al. [30] derived a semi-empirical relation for predicting the second-order index of refraction, n_2, for semiconductors from the linear refractive index, n which has the simplest form:

$$n_2(\times10^{-13}esu) = G\frac{n-1}{v_d^{5/4}} \tag{14}$$

where G is an empirical constant   ($G{=}391$) [31] and v_d is the Abbe dispersion number and is given by:

$$v_d = \frac{n_d-1}{n_F-n_C} \tag{15}$$

where n_d, n_F, and n_C refer to refractive indices at 589.0, 486.1, and 656.3 nm respectively.

The two-photon absorption coefficient β is given by [31]:

$$\beta = \frac{KE_p^{1/2}F(2h\nu/E_g)}{n^2E_g^3} \tag{16}$$

where K is the material-independent constant. In our calculations, $K = 3100$ and E_P is related to the Kane momentum parameter, p, where $E_P = 2p^2m/h^2$ and m is the electron mass. F is a function which represents the dispersion of β with respect to the incident photon energy $h\nu$. This function depends upon the band structure and determines the energy states that are coupled. The function F can be evaluated from the relation [32]:

$$F(2h\nu/E_g) = \frac{[(2h\nu/E_g)-1]^{3/2}}{(2h\nu/E_g)^5} \tag{17}$$

According to the dispersion behavior of β, shown in Figure 9a, a ratio between the maximum nonlinear absorption coefficients of the two photon absorption (TPA) to the optical bandgap energy equals to 1.4 is observed for different chalcogenide compositions [36-39]. The maximum nonlinear absorption coefficient β for investigated films, are given in Table 3, The dispersion of $n_2{=}f(h\nu)$ are plotted as shown in Figure 9b.

Table 3.   The nonlinear Absorption Coefficient, β_{max}, Values of the Energy Corresponding to β_{max}, $E_{\beta=max}$, Ratio of $E_g/E_{\beta=max}$ for the Studied Samples

Film Composition	β_{max} cm/GW	$E_{\beta=max}$ eV	$E_g/E_{\beta=max}$
a-Se	13.6006	1.4739	1.42
c-SeDy$_{0.008}$	16.7625	1.3805	1.42
c-SeDy$_{0.01}$	26.631	1.1197	1.42
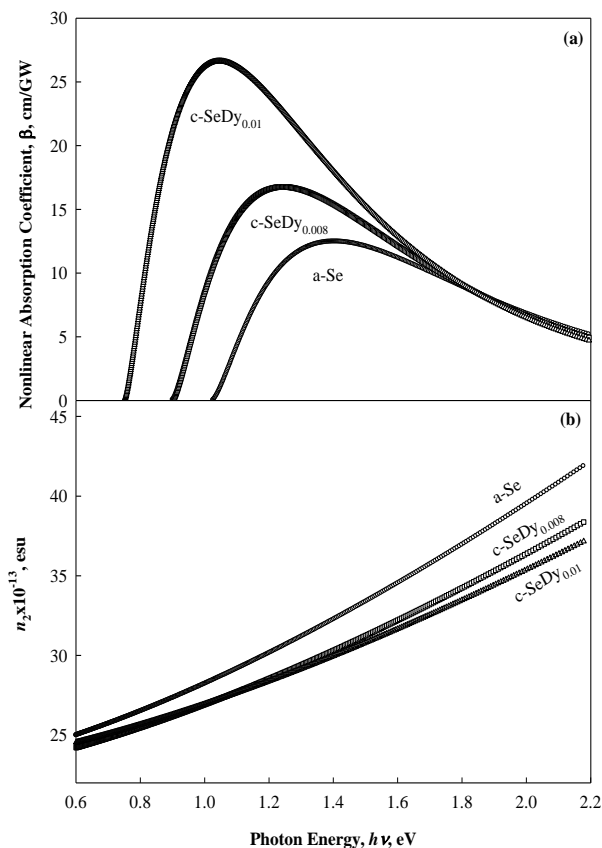
Figure 9. Dependence of nonlinear absorption coefficient, β (a) and second order refractive index, n_2 (b) on the incident photon energy, $h\nu$ for the studied films

4. Conclusions

The study of the role played by dysprosium ions as a dopant in the structural network of a-Se on optical dispersion leads to draw the main following concluding remarks:

- Doping of a-Se with Dy rare earth ions assist the crystalline phase to grow on the expense of amorphous phase.
- The optical band gap (E_g) decreases with increase of the Dy content which is argued to the difference in electronegativity between Se and Dy and change of part of amorphous phase to crystalline one.
- The variance between the values of the optical energy gaps of the studied samples and previously published data for other chalcogenide compositions doped also with Dy are attributed to the sensitivity of chalcogenides to its thermal history and preparation conditions.
- The single oscillator energy, E_0, showed a decrease accompanied by an increase in the values of E$_d$. This trend of E_0 and E_d shifted the material dispersion $M(\lambda)$ towards longer wavelengths from 1.6 to 1.74 μm against the increase in the Dy-content. This shift means that the material dispersion of chalcogenide fiber could be tuned by controlling the doping ratio of Dy.

- A ratio between the maximum nonlinear absorption coefficients of TPA to the optical bandgap energy equals to 1.4 is observed for different chalcogenide semiconductors.

REFERENCES

[1]   C. Liu, and J. Heo, "Generation of white light from oxy-fluoride nano-glass doped with Ho^{3+}, Tm^{3+} and Yb^{3+}," Mater. Lett., vol. 61, pp. 3751-3754, Jul. 2007.

[2]   Q. Su, H. Liang, C. Li, H. He, Y. Lu, J. Li, and Y. Tao, "Luminescent materials and spectroscopic properties of Dy^{3+} ion," J. Lumin., vol. 122, pp. 927-930, Jan. 2007.

[3]   G. Tang, Z. Yang, L. Luo, and W. Chen, "Dy $^{3+}$-doped chalcohalide glass for 1.3-μm optical fiber amplifiers," J. Mater. Res., vol. 23, pp. 954-961, Apr. 2008.

[4]   N. F. Mott, and E. A. Davis, "Electronic processes in non-crystalline materials," Oxford University Press, Oxford, Fab. 2012.

[5]   S. R. Elliott, "Physics of amorphous materials," Longman Group, Longman House, Burnt Mill, Harlow, Essex CM 20 2 JE, England, 1983.

[6]   A. Zakery, and S. R. Elliott, "Optical nonlinearities in chalcogenide glasses and their applications," Vol. 135, Berlin, Springer, Jan. 2007.

[7]   B. J. Park, H. S. Seo, J. T. Ahn, Y. G. Choi, J. HEO, and W. J. Chung, "Dy^{3+} doped Ge-Ga-Sb-Se glasses and optical fibers for the mid-IR gain media," J. Ceram. Soc. Japan, vol. 116, pp. 1087-1091, 2008.

[8]   J. Heo, "Rare-earth doped chalcogenide glasses for fiber-optic amplifiers," J. Non-Cryst. Solids, vol. 326, pp. 410-415, Oct. 2003.

[9]   Y. Shen, Y. M. Li, Q. G. Hu, W. Q. Luo, and Z. M. Wang, "Dielectric properties of B–site charge balanced Dy–doped SrTiO$_3$ ceramics for energy storage," J. Electroceram., vol. 34, pp. 236-240, Jun. 2015.

[10] F. A. Abdel-Wahab, and H. A. Maksoud, "Electrical conduction and dielectric relaxation in selenium films doped with dysprosium rare earth," Am. J. Cond. Matter. Phys., vol. 7, pp. 41-49, 2017.

[11] V. Pamukchieva, and A. Szekeres, "Optical properties of GexSb$_{20}$-xTe$_{80}$ thin films and their changes by light illumination," Opt. Mater., vol. 30, pp. 1088-1092, Mar. 2008.

[12] S. Boycheva, A. K. Sytchkova, J. Bulir, C. Popov, W. Kulisch, and A. Piegari, "Optical constants of As$_2$Se$_3$–Ag$_4$SSe–SnTe amorphous thin films," J. Non-Cryst. Solids, vol. 353, pp. 1618-1623, Jun. 2007.

[13] R. Swanepoel, "Determination of surface roughness and optical constants of inhomogeneous amorphous silicon films," J. Phys. E: Sci. Instrum., vol. 17, pp. 896-903, Oct. 1984.

[14] R. Swanepoel, "Determination of the thickness and optical constants of amorphous silicon," J. Phys. E: Sci. Instrum., vol. 16, pp. 1214-1222, Dec. 1983.

[15] M. Fox, "Optical Properties of Solids," Oxford University Press, New York, 2010.

[16] V. Nazabal, P. Němec, J. Jedelský, C. Duverger, J. Le Person, J. L. Adam, and M. Frumar, "Dysprosium doped amorphous chalcogenide films prepared by pulsed laser deposition," Opt. Mater., vol. 29, pp. 273-278, Nov. 2006.

[17] J. Tauc, R. Grigorovici, and A. Vancu, "Optical properties and electronic structure of amorphous germanium," Phys. Status Solidi (b), vol. 15, pp. 627-637, 1966.

[18] J. Tauc, "Optical properties of amorphous semiconductors. In amorphous and liquid semiconductors," Springer, Boston, MA, pp. 159-220, 1974.

[19] K. Sharma, M. LALb, and N. Goyal, "Optical properties of amorphous $Se_{80-x}Te_{20}Bi_x$ thin films," J. Optoelec. Biomed. Mater., vol. 6, pp. 27-34, Apr. 2014.

[20] F. Urbach, "The long-wavelength edge of photographic sensitivity and of the electronic absorption of solids," Phys. Rev., vol. 92, pp. 1324-1325, Dec. 1953.

[21] D. Redfield, "Energy-band tails and the optical absorption edge; the case of a-Si: H," Solid State Commun., vol. 44, pp.1347-1349, Dec. 1982.

[22] M. L. Theye, A. Gheorghiu, K. Driss-Khodja, and C. Boccara, "Absorption edge in amorphous Ge and GaAs: comparative study of the role of disorder and defects," J. Non-Cryst. Solids, vol. 77, pp. 1293-1296, Dec. 1985.

[23] T. S. Moss, C. J. Burrell and B. Ellis, "Semiconductor opto-electronics," Butterworth & Co. Ltd, New York, Dec. 1973.

[24] S. H. Wemple, and M. DiDomenico Jr., "Behavior of the electronic dielectric constant in covalent and ionic materials," Phys. Rev. B, vol. 3, pp.1338-1351, Feb. 1971.

[25] S. H. Wemple, "Material dispersion in optical fibers," Appl. Opt., vol. 18, pp. 31-35, Jan. 1979.

[26] H. Poignant, "Dispersive and scattering properties of a ZrF_4 based glass," Electron. Lett., vol. 17, pp. 973-974, Dec. 1981.

[27] K. Nassau, and S. H. Wemple, "Material dispersion slope in optical-fibre waveguides," Electron. Lett., vol. 18, pp. 450-451, May 1982.

[28] R.W. Boyd, "Nonlinear optics, "Academic press, USA, Jan. 2003.

[29] M. Klimczak, B. Siwicki, P. Skibiński, D. Pysz, R. Stępień, A. Heidt, C. Radzewicz, and R. Buczyński, "Coherent supercontinuum generation up to 2.3 µm in all-solid soft-glass photonic crystal fibers with flat all-normal dispersion," Opt. Express, vol. 22, pp. 18824-18832, Jul. 2014.

[30] L. Liu, T. Cheng, K. Nagasaka, H. Tong, G. Qin, T. Suzuki, and Y. Ohishi, "Coherent mid-infrared supercontinuum generation in all-solid chalcogenide microstructured fibers with all-normal dispersion," Opt. Lett., vol. 41, pp. 392-395, Jan. 2016.

[31] N.L. Boling, A. Glass, and A. Owyoung, "Empirical relationships for predicting nonlinear refractive index changes in optical solids," IEEE J. Quantum. Electron., vol. 14, pp. 601-608, Aug. 1987.

[32] F. A. Wahab, F. El-Diasty, and M. Abdel-Baki, "Dispersion dependence of second-order refractive index and complex third-order optical susceptibility in oxide glasses," Phys. Lett. A, vol. 373, pp. 3855-3860, Oct. 2009.

[33] C. Quémard, F. Smektala, V. Couderc, A. Barthelemy, and J. Lucas, "Chalcogenide glasses with high nonlinear optical properties for telecommunications," J. Phys. Chem. Solids, vol. 62, pp. 1435-1440, Aug. 2001.

[34] F. Smektala, C. Quemard, L. Leneindre, J. Lucas, A. Barthélémy, and C. De Angelis, "Chalcogenide glasses with large non-linear refractive indices," J. Non-Cryst. Solids, vol. 239, pp.139-142, Oct. 1998.

[35] R. Rangel-Rojo, K. Kimura, H. Matsuda, M. A. Mendez-Rojas, and W. H. Watson, "Dispersion of the third-order nonlinearity of a metallo-organic compound," Opt. Commun., vol. 228, pp.181-186, Dec. 2003.

[36] L. Petit, N. Carlie, R. Villeneuve, J. Massera, M. Couzi, A. Humeau, G. Boudebs, and K. Richardson, "Effect of the substitution of S for Se on the structure and non-linear optical properties of the glasses in the system $Ge_{0.18}Ga_{0.05}Sb_{0.07}S_{0.70-x}Se_x$," J. Non-Cryst. Solids, vol. 352, pp. 5413-5420, Dec. 2006.

[37] A. Zakery, and S. R. Elliott, "Optical properties and applications of chalcogenide glasses: a review," J. Non-Cryst. Solids, vol. 330, pp. 1-12, Nov. 2003.

[38] K. Petkov, and P. J. S. Ewen, "Photoinduced changes in the linear and non-linear optical properties of chalcogenide glasses," J. Non-Cryst. Solids, vol. 249, 150-159, Jul. 1999.

[39] J. Requejo-Isidro, A. K. Mairaj, V. Pruneri, D. W. Hewak, M. C. Netti, and J. J. Baumberg, "Self refractive non-linearities in chalcogenide based glasses," J. Non-Cryst. Solids, vol. 317, pp. 241-246, Mar. 2003.